International Journal for Housing Science and Its Applications
Publish August 10, 2025. Volume 46, Issue 4 Pages 2399-2409

https://doi.org/10.70517/ijhsa464203

Flow dynamics and heat transfer of cigarette smoke based on computational fluid dynamics

Wanpeng Sun[1,*], Yaxin Li[1], Huapeng Cui[2], Xuehui Sun[2], Cong Nie[2] and Jizhao Guo[2]
[1] School of Chemistry and Chemical Engineering, Henan University of Technology, Zhengzhou, Henan, 450001, China
[2] Zhengzhou Tobacco Research Institute, Zhengzhou, Henan, 450001, China
Corresponding authors: (e-mail: wpsun@haut.edu.cn).

Abstract In recent years, new types of cigarettes featuring innovative designs and materials have emerged. However, the complexity of their composition, structure, and components has led to an unclear understanding of the flow and transmission processes of aerosol within the smoke. There is an urgent need to utilize new technologies, such as computational fluid dynamics (CFD), to conduct in-depth research on these processes in cigarettes. This paper establishes a three-dimensional model of the flow and transmission of smoke aerosol within a cigarette, based on the fundamental parameters of a typical cigarette and the basic physical properties of smoke aerosol. Through this model, we simulate and analyze the flow states and temperature field distributions of various typical cigarette smoke aerosols, exploring the impacts of cigarette structure, ventilation filter design, and pressure drop distribution of smoke aerosol during the smoking process on the temperature field distribution. This research lays a solid foundation for constructing and enhancing the risk assessment system for Chinese tobacco products.

Index Terms computational fluid dynamics, cigarette smoke, pressure drop, temperature distribution

I. Introduction

As the country with the largest number of smokers in the world, smoking-related diseases have caused enormous harm to the health of the Chinese people and significant losses to economic and social development. Therefore, in-depth research on cigarette smoke composition and transmission, as well as the development of technologies for tar reduction and harm reduction in cigarettes, has become a major focus in the industry. When a cigarette is ignited, combustion generates a smoke aerosol composed of thousands of gaseous and solid substances, forming a complex aerosol system [1], [2]. During cigarette combustion, the flow and transport of smoke aerosols involve complex processes, including the combustion and pyrolysis chemical reactions of tobacco and the momentum, heat, and mass transfer between the smoke and the tobacco [3]-[5]. The gas flow field during this process directly affects the temperature distribution within the cigarette, which in turn determines the generation of harmful components such as nicotine, tar, and carbon monoxide, as well as the ratio, transformation, and mass transfer processes between the particulate and gaseous phases. Consequently, the flow field distribution of smoke aerosol transport inside cigarettes has gradually become a research focus in this field [6].

Computational Fluid Dynamics (CFD), an interdisciplinary technology that solves fluid dynamics control equations through numerical methods to obtain discrete quantitative descriptions of flow fields and predict fluid behavior, can be applied to study smoke aerosol transport in cigarettes, providing critical information such as smoke flow velocity and airflow field distribution that is difficult to obtain experimentally [7]. In recent years, the numerical simulation and modeling of smoke aerosol transport inside cigarettes based on CFD have flourished. As early as 1976, Baker et al. studied the smoke flow and transport processes during cigarette combustion and analyzed the airflow field distribution around the burning cone using Darcy's Law [8]. Eitzinger et al. combined conservation laws, porous media fluid dynamics theory, and Darcy's Law to study the effects of cigarette cover materials (such as tipping paper, cigarette paper, filter tips, and tobacco rods) on filter ventilation and draw resistance, investigating the anisotropic, non-uniform, and nonlinear behaviors in the constitutive equations, which provided valuable guidance for CFD parameter settings in simulations [9]. Wang Le et al. constructed a three-dimensional mathematical model of smoke flow through the entire cigarette by measuring pressure drop and total ventilation rate under various puffing conditions without combustion, and used it to analyze pressure drop and flow rate distribution under constant velocity and ISO standard puffing conditions for 3R4F cigarettes. Their results showed that airflow inside non-burning cigarettes could be described using Darcy's Law, with numerical simulations closely matching experimental results [10]. Yu Qichang et al. combined CFD technology with Particle Image Velocimetry (PIV) to study the radial diffusion of cigarette smoke through cigarette paper and the axial flow of smoke from the lit end to the mouth end,

obtaining the distribution of CO as a representative smoke component inside the cigarette [11]. Due to the complex composition, structure, and components of cigarettes, the smoke aerosol transport process is influenced by multiple factors, highlighting the urgent need for further in-depth research using new technologies like CFD.

During cigarette combustion, components such as tobacco, cigarette paper, and structural features of the cigarette all influence smoke flow and the internal temperature distribution. Gugan was the first to study the internal temperature distribution of cigarettes in the 1960s, establishing a diffusion-controlled smoldering model and obtaining some basic characteristics of cigarette internal temperature profiles [12]. Muramatsu et al. proposed a one-dimensional mathematical model of temperature and density changes in the evaporation-pyrolysis zone of naturally burning cigarettes, predicting the smoldering rate and temperature distribution, although this model only considered tobacco evaporation and pyrolysis reactions, without addressing combustion under low-oxygen conditions [13]. Yan Cong et al. used CFD and Fluent software to simulate the smoldering process of cigarettes, including water evaporation, tobacco pyrolysis and oxidation reactions, as well as mass, energy, and momentum transfer. They analyzed temperature distributions at different time points and the concentration distributions of oxygen, carbon monoxide, carbon dioxide, and water vapor in the smoke. Their simulated linear burning rates (LBR) and maximum smoldering temperatures closely matched experimental values [14]. Chen, in analyzing cigarette combustion and pyrolysis processes, divided cigarettes into combustion and pyrolysis zones by defining a receding combustion front and built a mathematical model capable of simultaneously simulating pyrolysis and oxidation. This model predicted the burning rate, length of the char zone, and maximum temperature in the oxidation zone, showing good agreement with experimental data [15].

In recent years, as market competition has intensified, cigarette products must continuously innovate in terms of specifications, filter materials, and designs. However, much of this innovation relies on empirical perception and sensory evaluation, lacking theoretical support [16], [17]. Studies at home and abroad have shown that experimental methods to measure, record, and analyze smoke aerosol flow inside cigarettes face limitations such as low equipment precision, long research cycles, and lack of theoretical foundations [18], [19]. In contrast, CFD-based numerical simulation methods for studying smoke aerosol transport inside cigarettes offer advantages such as fewer model constraints, a wide range of adjustable parameters, and intuitive visualization of internal smoke aerosol flow states [20], [21].

Therefore, this study aims to experimentally determine the basic parameters and physical properties of smoke aerosols in a series of typical cigarettes, establish a three-dimensional CFD model of smoke aerosol flow inside the cigarette, and systematically investigate the effects of cigarette specifications, smoking process, puffing patterns, and ventilated filter tip structures on smoke aerosol flow and heat transfer during smoking. This will reveal the flow states and temperature distributions of smoke aerosols in typical cigarettes during smoking, providing theoretical foundations and data support for the design and optimization of new cigarette products.

II. Experimental Material Design and Parameter Measurement

II. A.Experimental Materials, Reagents, and Instruments

Different specifications of 3R4F standard cigarettes (Henan China Tobacco Industry Co., Ltd.), scissors, tweezers. Electronic balance (BS 323S, sensitivity: 0.0001 g, Sartorius Instrument Systems Co., Ltd., Beijing). Mercury porosimeter (AUTOPORE 9510, USA, pore size measurement range: 3 nm–350 μm). Single-channel smoking machine (SML100, China, Anhui). Temperature measuring instrument (DATAPAQ-Q18, UK, measurement range: -200 ℃ to 1370 ℃).

II. B.Measurement of Tobacco and Filter Rod Porosity

The cigarette samples were separated into tobacco rod and filter sections, dried in a 105 ℃ oven for 2 hours, and then ground into powder for use. The electronic balance was used to measure the mass of the powder expansion meter and the combined mass after adding the powdered sample to determine the sample mass under vacuum conditions. Subsequently, the mercury porosimeter was employed to test the samples, and the porosity of both tobacco and filter rods was calculated accordingly.

II. C.Measurement of Resistance Characteristics of Cigarette Rods and Filters

A series of cigarette samples (with circumferences of 24 mm, 20 mm, and 17 mm) were fixed into the smoking machine. The vacuum pump was activated to simulate ISO standard puffing and deep puffing processes. Using a high-precision differential pressure meter, the pressure drop parameters of the cigarette samples under different puffing modes were measured.

II. D.Measurement of Cigarette Combustion Temperature

A high-precision thermocouple was inserted into the burning cigarette rod (circumferences: 24 mm, 20 mm, and 17 mm). The ISO standard puffing process and deep puffing process were simulated using the smoking machine, and the temperature distribution of the burning cone during combustion under different puffing modes was recorded.

III. Numerical Simulation Methods

III. A. Physical Model

The acetate fibers inside the tobacco rod and the filter of typical cigarettes are bundled structures.

These fiber bundles overlap each other, resulting in irregular and disordered channels for smoke flow within the cigarette rod and filter. Under both ISO standard puffing and deep puffing modes, the gas flow velocity inside the cigarette rod remains low, with Reynolds numbers below 3000, indicating laminar flow behavior following Darcy's Law. Therefore, a series of assumptions and simplifications are made when conducting numerical simulations using computational fluid dynamics (CFD):

(1) The smoke aerosol flowing inside the cigarette rod during combustion is treated as an incompressible fluid.

(2) The cigarette paper and tobacco are considered porous media with uniform and constant pore sizes.

(3) The tipping paper and acetate fiber filter are treated as porous media with uniform and constant pore sizes.

The continuity equation and momentum equation governing the fluid flow process are as follows:

$$\nabla \cdot \vec{u} = 0 \tag{1}$$

$$\frac{\partial}{\partial t}(\rho \vec{u}) + \nabla \cdot (\rho \vec{u}\vec{u}) = -\nabla p + \nabla \cdot (2\mu \vec{N}) + \vec{F}_s + \rho g \tag{2}$$

ρ is the density (kg/m3), μ is the dynamic viscosity (Pa·s), p is the pressure (Pa), $\vec{u}$ is the fluid velocity (m/s), $\vec{N}$ is the stress tensor(m/s2), $\vec{F}_s$ is the body force caused by surface tension (m/s2).

III. B. Geometric Model

Based on the 3R4F standard cigarette and reasonable simplifications, a three-dimensional geometric model of the cigarette was established, as shown in Figure 1. Taking a typical conventional cigarette as an example, the total length of the cigarette is 84 mm, with a tobacco rod length of 60 mm and a filter segment length of 24 mm. The circumference of the cigarette is 24 mm, corresponding to a diameter of 7.9 mm. Based on the cylindrical structure of the cigarette, a multi-region meshing approach was employed. Considering the requirements for computational accuracy and efficiency, and after mesh independence verification, the minimum mesh size was set to 0.2 mm, resulting in approximately 693,000 total mesh elements.

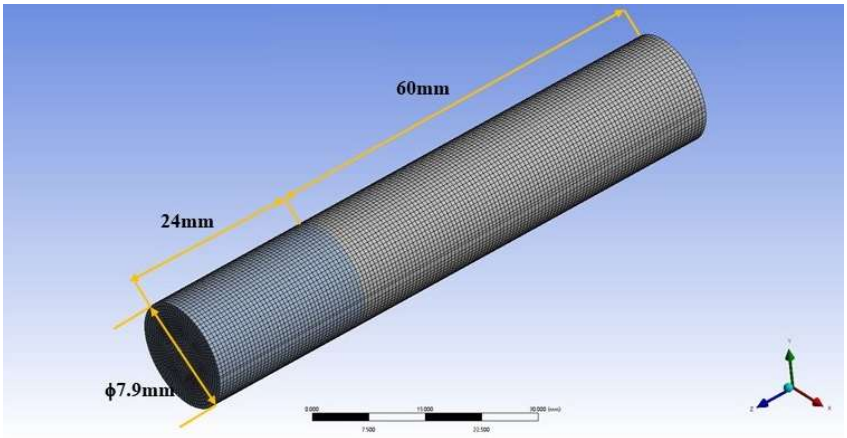

Figure 1: Schematic diagram of geometric model and mesh division of cigarette

III. C. Boundary Conditions

When the 3R4F standard cigarette is smoked under the ISO standard puffing regime, the puff flow rate is 17.5 mL/s, the duration of each puff is 2 seconds, and the total volume per puff is 35 mL. Previous studies have shown that during smoking, the tobacco, cigarette paper, and other components combust together, forming a combustion cone at the front end of the cigarette. The maximum temperature of this combustion cone can exceed 1000 °C, with an average temperature above 430 °C. Tobacco pyrolysis begins at temperatures above 200 °C, and after the smoke passes through the pyrolysis zone, its temperature drops below 200 °C. Therefore, in the fluid dynamics simulation, it is considered scientifically reasonable to set the initial temperature of the smoke entering the tobacco rod after

the combustion cone at 200 °C. During the puffing process of the 3R4F standard cigarette, the cigarette is maintained at room temperature (298.15 K) and standard atmospheric pressure. The tobacco rod section is set as the smoke inlet with a velocity inlet condition, while the filter section is set as the smoke outlet with a pressure outlet condition.

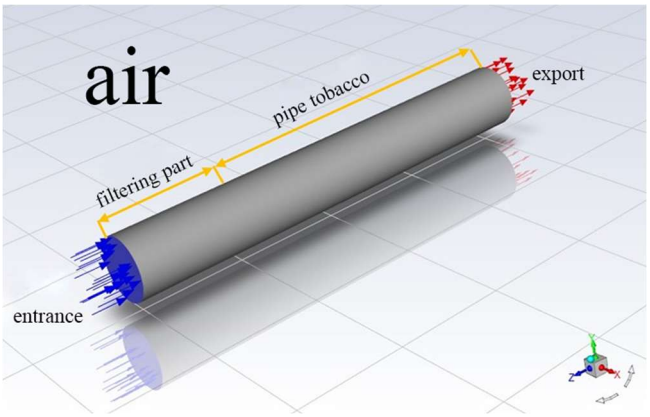

Figure 2: Schematic diagram of boundary conditions for cigarette model

(1) The cigarette inlet adopts a velocity inlet, with the inlet flow velocity set at 0.3889 m/s and the inlet temperature of the smoke set to 200°C (473.15 K).

(2) The filter outlet adopts a pressure outlet, with the static pressure at the outlet set to -1200 Pa and the outlet temperature set to room temperature, 25°C (293.15 K).

(3) Wall conditions: The side wall of the cigarette is set as a no-slip wall.

(4) Flow region conditions: The tobacco rod section and the filter section are set as different porous media regions. The porosity, viscous resistance coefficient, and inertial resistance coefficient of the tobacco and filter are not the same. The heat transfer rate is directly influenced by the specific heat capacity and thermal conductivity of the materials, which also differ significantly between the tobacco and filter materials. The specific parameters used in the computational fluid dynamics (CFD) numerical simulation model are shown in Table 1.

Table 1: Parameters of Fluid Dynamics Numerical Simulation Model

Sample	Geometric conditions	Parameter	Sample	Physical characteristics	parameter
1	Cigarette circumference	26mm, 24mm, 22mm, 20mm, 17mm	1	Density of tobacco segments	1100kg/m3
2	Cigarette diameter	8.4mm, 7.9mm, 7.0mm, 6.4mm, 5.4mm	2	Specific heat capacity of tobacco segments	2080J/(kg·K)
3	Length of tobacco segments	60mm, 53mm, 46mm, 39mm, 32mm, 25mm, 18mm, 11mm, 4mm	3	Thermal conductivity of the tobacco segment	0.024W/(m·K)
4	Filter segment length	24mm	4	Tobacco segment viscous resistance coefficient	7.13×108m-2
5	Diameter of the hollow section of the filter	6mm 4mm 2mm	5	Tobacco segment inertia drag coefficient	1.52×104m-1
6	Hollow section depth in the filter	10mm	6	Tobacco segment porosity	0.75
			7	Filter segment density	1300kg/m3
			8	Specific heat capacity of the filter section	1500J/(kg·K)
			9	Thermal conductivity of the filter segment	0.05W/(m·K)
			10	Coefficient of viscous resistance of the filter segment	6.94×109m-2
			11	Coefficient of inertial drag of the filter segment	0m-1
			12	Filter segment porosity	0.87

III. D. Solution Setup

The geometric model construction, mesh generation, and solution of the computational fluid dynamics (CFD) numerical simulation are all completed using Ansys Fluent 2022. Based on the unstable state of gas flow during the burning process, the flow of smoke and heat transfer within the cigarette is simulated using a three-dimensional unsteady laminar flow model. The pressure-velocity coupling equations are solved using the SIMPLE algorithm. Both pressure and momentum discretization are performed using a second-order upwind scheme, and the time step size is set to 0.0001 s.

IV. Results

IV. A. Smoke Flow and Heat Transfer During the Smoking Process of 3R4F Standard Cigarette in the Burning State

When the 3R4F standard cigarette is smoked in the ISO standard mode, each puff lasts for 2 seconds, followed by a static combustion period of 60 seconds, during which the cigarette burns approximately 7 mm. To further analyze the burning behavior under the ISO standard mode, the cigarette's burning condition is simulated by assuming that for each puff, the tobacco segment loses 7 mm, while the length of the filter section remains unchanged. The smoke flow and heat transfer within the cigarette are simulated after the first to sixth puffs (with cigarette lengths of 84 mm, 77 mm, 70 mm, 63 mm, 56 mm, and 49 mm, respectively). After 2 seconds of puffing, the pressure distribution inside the cigarette after the first to sixth puffs is shown in Figure 3.

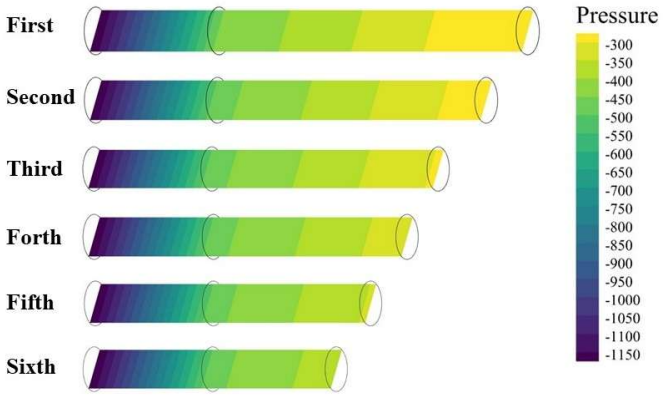

Figure 3: Internal pressure drop during cigarette combustion in ISO standard mode

From the figure, it can be seen that there is a uniform pressure drop gradient distribution in both the tobacco segment and the filter segment. However, they show significant differences. The pressure drop gradient in the tobacco segment is larger, while in the filter segment, the gradient is smaller. This can be attributed to the differences in materials between the tobacco and filter segments, as well as the substantial difference in porosity and resistance coefficients. These differences lead to varying flow resistance for the smoke as it travels through the same distance. The resistance in the filter segment is much higher, resulting in a smaller and more concentrated pressure drop gradient. Therefore, during the smoking process of the cigarette, the pressure drop in the tobacco segment remains relatively constant, ranging from 400 to 500 Pa during the first puff. Afterward, as the smoking continues and the tobacco segment burns shorter, the resistance in the tobacco segment decreases, which in turn reduces the pressure drop, reaching about 200 to 250 Pa by the sixth puff. In contrast, since the length of the filter segment does not change, the pressure drop in the filter segment does not change significantly as the number of puffs increases.

During the smoking process of the 3R4F standard cigarette, the hot gas flows through the cigarette, transferring heat with the tobacco and filter segments, potentially accompanied by thermal radiation and convection, as well as phase changes such as evaporation, sublimation, and condensation of various components in the smoke. Therefore, the temperature distribution of the hot gas along the entire cigarette during its flow is crucial for cigarette research. In the ISO standard mode, after different numbers of puffs, the temperature distribution of the smoke at the central axis of the cigarette is shown in Figure 4.

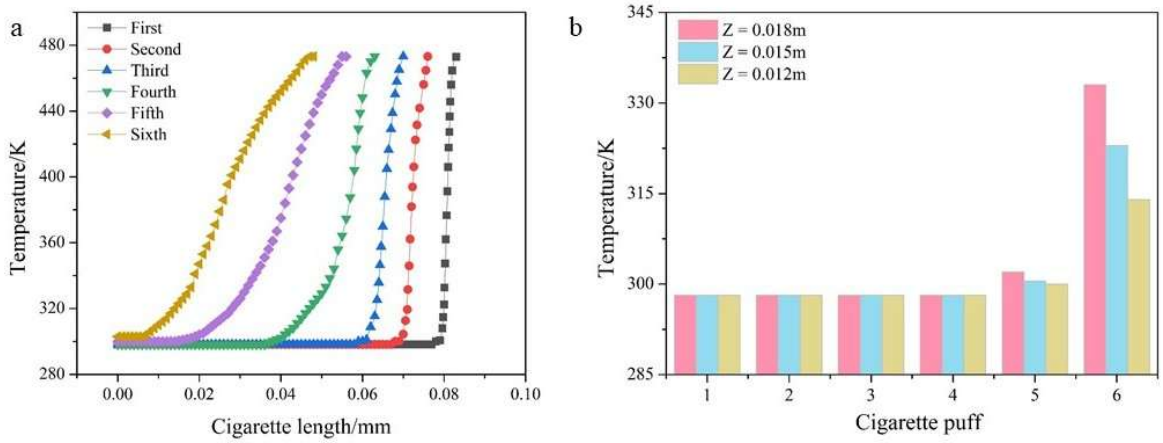

Figure 4: (a) Temperature distribution inside the cigarette during combustion in ISO standard mode, (b) Temperature comparison at the center of the cigarette combustion axis (Z=0.018m, Z=0.015m) with per puff in ISO standard mode

From Figure 4a, it can be observed that when the cigarette is smoked during the first puff, the cigarette length remains unchanged, and the temperature inside the cigarette rapidly drops from the highest temperature of 200°C (473.15 K) to near room temperature (25°C) at a distance of 5-8 mm from the smoke inlet. The effect of the hot gas on the cigarette is limited, and the temperature distribution range at the front end of the cigarette is relatively small. The temperature of the smoke at the filter end remains at room temperature (25°C). As the cigarette undergoes smoking, the tobacco segment length decreases, the resistance to gas flow decreases, and the flow of smoke accelerates. When the cigarette length reduces to 53 mm, the temperature distribution gradient at the front end of the cigarette increases, and the affected temperature field extends to a range of 10-15 mm. At the same time, as the tobacco segment shortens with burning, the average temperature of the tobacco segment increases, but the rise is relatively small. Additionally, since the filter segment is still some distance away from the temperature field, its average temperature does not change significantly. By the time the sixth puff is taken, the tobacco segment length has decreased by 35 mm, which is more than half of the tobacco segment length. The resistance in the tobacco segment decreases significantly, and the temperature in the tobacco segment rises noticeably. The range of the temperature field expands further and even starts to affect the filter segment, with the temperature at the filter end reaching 30°C (303 K).

By comparing the temperature changes at different positions in the filter segment with the number of puffs, a more intuitive discussion can be made regarding the change in smoke temperature during the ISO smoking process of the 3R4F standard cigarette. Therefore, the temperature at the axial positions 0.012 m, 0.015 m, and 0.018 m from the filter end is selected to compare the variation with the number of puffs, as shown in Figure 4b. During the six puffs, the temperature at the three positions in the filter segment remains at room temperature (25°C) after the first four puffs, and the temperature at the filter outlet also remains at 25°C. This result indicates that after the first four puffs, the filter segment outlet temperature stays at room temperature and does not affect the smoking experience. Starting from the fifth puff, the smoke temperature in the filter segment begins to rise, with a significant increase between the fifth and sixth puffs. At the 0.018 m position from the filter outlet, the temperature reaches 60°C (333 K), and at the 0.015 m position, it reaches 50°C (323 K). This result is consistent with the temperature distribution findings from Li et al.'s study, confirming the accuracy of the model used in this research [22]. This result shows that, in the ISO smoking mode, the smoking experience during the first four puffs of the 3R4F standard cigarette does not change significantly. Starting from the fifth puff, the influence of the hot smoke gradually extends to the filter segment, and the smoking experience is gradually affected after the sixth puff.

IV. B. Smoke Flow and Heat Transfer in the Combustion Process of 3R4F Standard Cigarette Under Deep Inhalation of HCl

In the case of deep inhalation with HCl in the 3R4F standard cigarette, each puff has a volume of 50 mL, with each puff lasting 2 seconds, followed by a static burn for 60 seconds. To compare the differences in the combustion of the cigarette under the ISO standard puffing mode and the deep inhalation HCl puffing mode, the loss of 7 mm per puff is assumed for both modes. The smoke flow and heat transfer inside the cigarette are simulated for the deep inhalation HCl mode, with the cigarette length reduced after each puff (84 mm, 77 mm, 70 mm, 63 mm, 56 mm, and

49 mm) for the first through sixth puffs. After 2 seconds of inhalation, the pressure distribution inside the cigarette after the first through sixth puffs is shown in Figure 5.

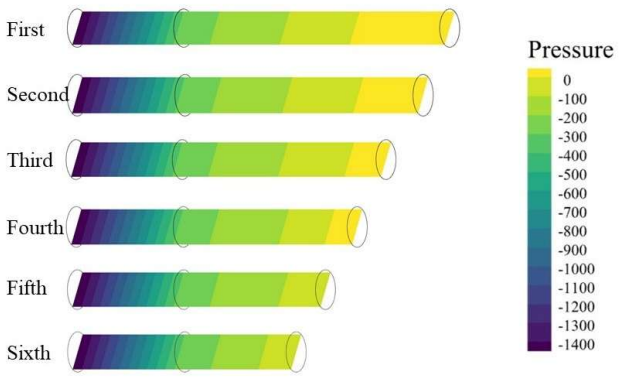

Figure 5: Internal pressure drop during cigarette combustion in HCI deep suction mode

From Figure 5, it can be observed that in the HCI deep inhalation mode, there is a uniformly distributed pressure drop gradient inside the cigarette. However, the pressure drop gradients in the tobacco rod and filter sections differ significantly, with the pressure drop gradient in the tobacco rod being relatively larger. This pressure drop gradient distribution is similar to that in the ISO standard puffing mode (as shown in Figure 3), which can also be attributed to the differences in resistance between the two materials.

In the HCI deep inhalation mode, during the first puff of the smoking process, the pressure drop in the tobacco rod remains around 400–500 Pa. Subsequently, as puffing continues, the pressure drop in the tobacco rod decreases, reaching approximately 250–300 Pa by the sixth puff. In contrast, the pressure drop in the filter section does not change significantly throughout the puffing process. This trend is generally similar to the pressure drop change trend in the ISO standard puffing mode. However, compared to the ISO standard mode, due to the overall increase in smoke flow in the HCI deep inhalation mode, the overall pressure drop in the cigarette increases by approximately 200–300 Pa for the same length, with the filter section contributing a larger proportion to the total pressure drop due to its higher resistance coefficient.

The HCI deep inhalation mode significantly increases the puffing volume compared to the ISO standard mode, and this has a significant impact on the temperature distribution inside the cigarette during the smoking process. Therefore, as shown in Figure 6, the temperature distribution at the axis of the 3R4F standard cigarette after different numbers of puffs in the HCI deep inhalation mode is examined to explore the evolution of the temperature field inside the cigarette.

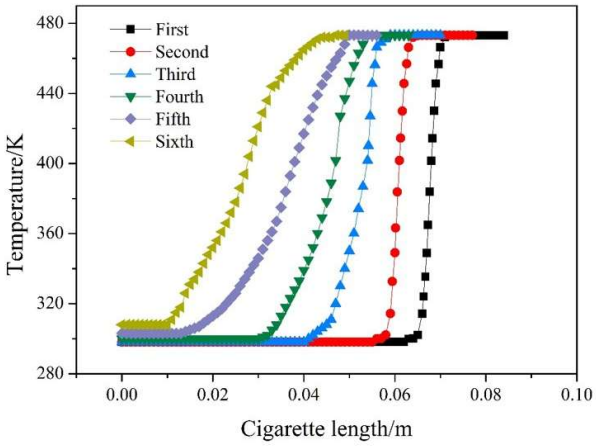

Figure 6: Temperature distribution inside cigarettes during combustion in HCI deep suction mode

Compared to the ISO standard puffing mode, after the first puff in the HCI deep inhalation mode, the smoke flow velocity inside the cigarette significantly increases, and the pressure drop increases notably. At a distance of 10–15

mm from the smoke inlet, the temperature of the smoke rapidly drops from a maximum of 200°C (473.15K) to near room temperature (25°C). The temperature field of the hot smoke affects a wider range, but the smoke temperature at the cigarette filter remains at room temperature (25°C). Due to the smoking process shortening the tobacco rod and reducing resistance, the impact range of hot smoke near the smoke inlet continues to expand. When the cigarette length decreases to 53 mm, the temperature field extends from 17 to 22 mm, and the average temperature in the tobacco rod increases slightly as the tobacco rod shortens. However, the average temperature in the filter section does not show a significant increase compared to the first puff. By the time the sixth puff is taken, the tobacco rod length has reduced by more than half of its original length, and the impact of the hot smoke on the tobacco rod increases significantly. The temperature field gradually extends to the filter section, with the filter outlet temperature rising further to 35°C (308K).

Based on the temperatures at the 0.015 m and 0.018 m axial positions from the filter outlet, the smoke temperature changes in the 3R4F standard cigarette under the ISO standard puffing mode and HCI deep inhalation mode were compared, as shown in Figure 7. Unlike the ISO standard puffing mode, in the HCI deep inhalation mode, after the fourth puff, the temperatures at both positions are around 27°C, and the filter outlet temperature is also 27°C. This indicates that due to the significantly increased smoke flow in the HCI deep inhalation mode, after the fourth puff, the filter outlet temperature begins to rise, gradually affecting the smoking experience. By the sixth puff, at the 0.018 m position from the filter outlet, the temperature in the HCI deep inhalation mode reaches about 70°C, and at 0.015 m, the temperature reaches about 58°C. This result is about 10°C higher than in the ISO standard puffing mode, indicating that due to the increased puffing flow, the smoking experience during the first three puffs in the HCI deep inhalation mode does not change significantly. However, starting from the fourth puff, the impact range of the hot smoke temperature field at the front of the cigarette gradually increases, and after the sixth puff, the smoking experience is significantly affected.

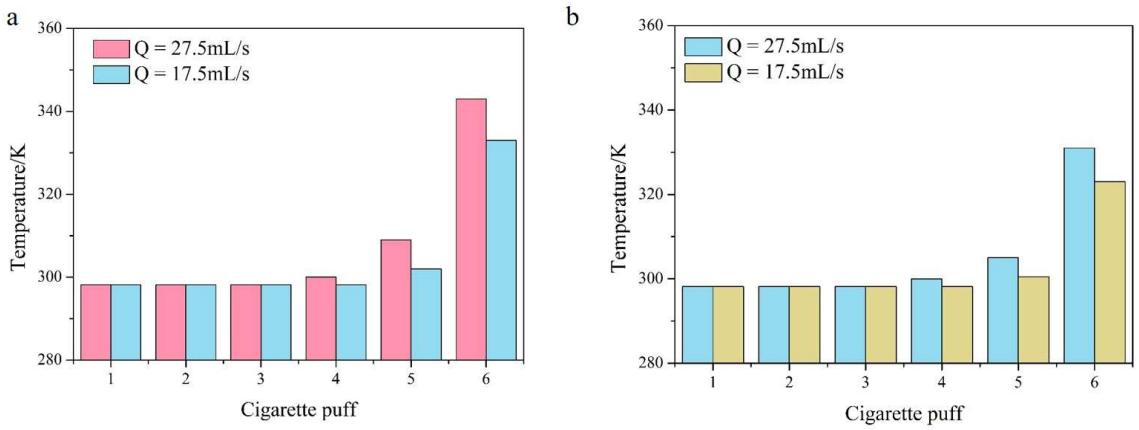

Figure 7: Temperature distribution at the center of the cigarette during combustion in ISO standard mode and HCI deep suction mode (a) Z=0.018m, (b) Z=0.015m

IV. C. The Smoke Flow and Heat Transfer During the Smoking Process of Cigarettes with Different Specifications

During cigarette design, the specifications of the cigarette, such as the circumference, the length of the tobacco rod, and the length of the filter, directly affect the gas flow velocity during the smoking process, which in turn influences the combustion cone at the cigarette's front end, causing changes in the smoker's sensory experience. Therefore, by analyzing the gas flow pressure distribution, heat transfer, and axial temperature within the cigarette after the same number of puffs under the ISO standard smoking mode, the effect of circumference on the smoking behavior of the standard cigarette is characterized. For different circumferences of the cigarette (17 mm, 20 mm, 22 mm, 24 mm, and 26 mm) under the ISO standard smoking mode, with 7 mm as the tobacco loss per puff, the gas flow pressure distribution in the cigarette after the sixth puff (49 mm) is shown in Figure 8.

Under the ISO standard smoking mode, all cigarettes with different circumferences exhibit a uniformly distributed pressure drop gradient inside (as shown in Figure 8). Similar to the 3R4F standard cigarette, the pressure drop gradient inside the straight cigarette shows a clear difference at the interface between the filter and tobacco rod, which fully demonstrates the significant impact of material resistance differences on the internal pressure distribution of the cigarette. Under the ISO standard smoking mode, the pressure drop in the tobacco rod of the slim cigarette

remains around 350–400 Pa, while as the circumference of the cigarette increases, the pressure drop in the tobacco rod decreases. When the circumference is 26 mm, the pressure drop is approximately 200–250 Pa. Similarly, the pressure drop in the filter section also decreases with an increase in the cigarette's circumference. This trend significantly differs from the variation in pressure drop with the number of puffs. This may be due to the reduction in internal resistance as the circumference of the cigarette decreases, which causes a significant increase in the gas flow velocity inside the cigarette compared to thicker cigarettes, and the corresponding pressure drop increases.

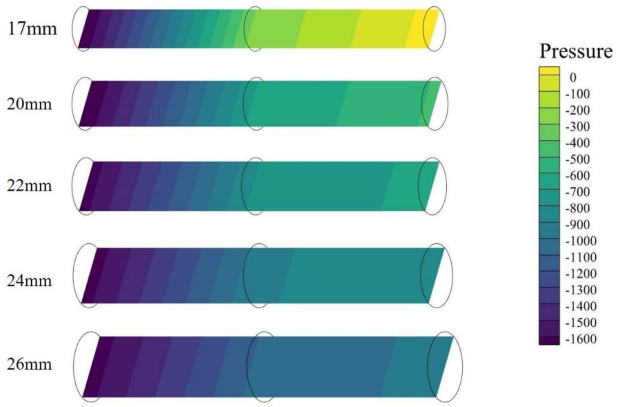

Figure 8: Internal pressure drop during combustion and inhalation of cigarettes with different circumferences in ISO standard suction mod

The impact of different circumferences on the internal pressure distribution of the cigarette also affects the gas flow inside the cigarette during the smoking process, which in turn leads to changes in the temperature distribution within the cigarette. Therefore, the distribution of gas temperatures at the axial positions of cigarettes with different circumferences under the ISO standard smoking mode is shown in Figure 9, which is used to explore the effect of circumference on the evolution of the temperature field inside the cigarette under the ISO standard smoking mode.

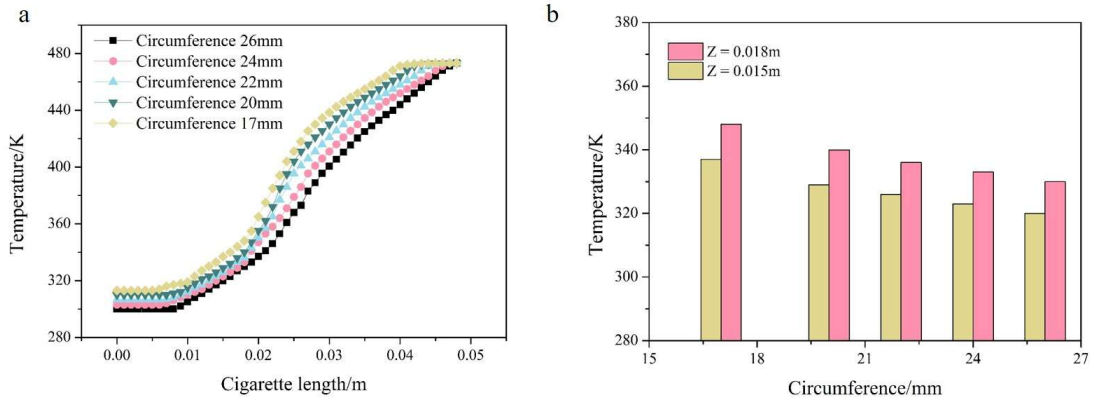

Figure 9: (a) Temperature distribution at the axis of cigarettes with different circumferences during combustion in ISO standard mode (b) Temperature comparison at the axis of cigarettes with different circumferences during combustion in ISO standard mode (Z=0.018m, Z=0.015m)

For slim cigarettes (17 mm), after the sixth puff, the gas flow speed inside the cigarette significantly increases, the pressure drop increases significantly, and the temperature field of the hot gas expands, with the temperature gradient range extending to the filter segment. The temperature at the filter outlet increases to 40°C. As the cigarette circumference increases, the internal resistance of the cigarette increases. At the same puff volume (35 mL), the gas flow speed inside the cigarette increases, and the effect range of the hot gas near the gas inlet decreases. When the cigarette circumference increases to 22 mm, the temperature field's influence range decreases by 3-5 mm, and the filter segment's outlet temperature drops to 33.5°C. When the cigarette circumference increases to 26

mm, the effect range of the hot gas on the cigarette is significantly reduced due to the circumference being more than 1/2 larger than the original size, and the filter segment's outlet temperature further decreases to around 27°C.

As shown in Figure 9b, under the ISO standard mode, the temperature at the axial positions 0.015 m and 0.018 m from the filter outlet has a negative correlation with the cigarette circumference. At a distance of 0.018 m from the filter outlet, as the cigarette circumference increases from 17 mm to 26 mm, the internal temperature decreases from 75°C to around 57°C. At a distance of 0.015 m from the filter outlet, as the cigarette circumference increases to 26 mm, the internal temperature decreases from 64°C to around 47°C. This also proves that as the cigarette circumference significantly increases, the overall internal temperature of the cigarette shows a negative correlation and gradually decreases. This result indicates that as the internal resistance of the cigarette increases with the larger circumference, the resistance to gas flow inside the cigarette increases, the flow speed decreases, and the influence range of the hot gas becomes smaller. The temperature field at the cigarette's front end narrows, its impact on the filter segment's temperature is limited, and the internal temperature of the filter segment and the outlet temperature both decrease, ultimately presenting a negative correlation between the smoking temperature and the cigarette circumference.

V. Discussion

This study is based on the fundamental parameters of 3R4F cigarettes, including the basic physical properties of materials such as tobacco and the filter, and through reasonable simplifications and assumptions, a three-dimensional numerical simulation model for the aerosol flow in a burning cigarette was developed. Using this model, the study explored the effects of the smoking process, smoking mode, and cigarette specifications on the flow and temperature field distribution of the aerosol during the smoking process. (1) Under the ISO standard smoking mode, as the smoking process progresses, the tobacco rod burns shorter, and its pressure drop decreases, while the pressure drop in the filter segment remains relatively unchanged due to its constant length. There is little change in the smoke temperature during the first four puffs, but from the fifth puff onward, the smoking sensation gradually changes. (2) Compared to the ISO standard smoking mode, the HCI deep puffing mode increases the overall gas flow, resulting in a 200-300 Pa increase in the overall pressure drop of the cigarette for the same length. Furthermore, in the smoking process, for the same length, the hot gas temperature at the front of the cigarette is more pronounced in the HCI deep puffing mode, causing an increase in the temperature at the filter outlet. (3) As the cigarette circumference increases, the internal resistance of the cigarette significantly increases, resulting in a corresponding increase in pressure drop. Consequently, the influence range of the hot gas decreases as the internal gas flow speed slows down, leading to a narrowing of the temperature field at the front of the cigarette. This results in a negative correlation between the smoking sensation temperature and the cigarette circumference. This study reveals the quantitative relationship between the flow state of the cigarette aerosol and the temperature field distribution, smoking process, smoking mode, and structural parameters, providing a foundation for the design and optimization of Chinese-style cigarettes.

Funding

This work was supported by the Science and Technology Foundation of Henan Province (No. 232102320084); the Open Project Program (No. 312021AW0420).

References

[1] SHOU Lan. A perspective on the current situation of China's cigarette market[J]. Economic Forum,2005(2): 34-36.
[2] DENG Qixin, XIE Wei, LIU Zechun, et al. Correlation between pH of total particulate matter and release of acidic and basic components in cigarette smoke[J]. Tobacco technology, 2021, 54(11): 13.
[3] WANG Xiaofeng, ZHANG Jin, CAO Yun, et al. Study on the correlation between cigarette combustion parameters, ash appearance and smoke composition[J]. Chinese Journal of Tobacco Science, 2022, 28(5): 17-22.
[4] WANG Hao, XIONG Bin, ZHOU Hongshen, et al. Research progress of fluorescence analysis technology in the detection of cigarette smoke components[J]. Physical and chemical examination (Chemical Division), 2014(12): 1609-1612.
[5] SONG Lingyong, ZHAO Qi, HUANG ShiJie, et al. Simultaneous determination of 15 phenolic components in mainstream cigarette smoke by gas Chromatography-Mass spectrometry[J]. Physical and Chemical Examination (Chemical Division), 2020, 56(10): 1085-1090.
[6] LI B, ZHAO L C, WANG L, et al. Gas-phase pressure and flow velocity fields inside a burning cigarette during a puff[J]. Thermochimica Acta, 2016, 623: 22-28.
[7] 2019.TANG Darong. Study on the flow state of cigarette smoke in filter based on CFD[D]. Guangdong: South China University of Technology, 2019.
[8] BAKER R R. Gas velocities inside a burning cigarette[J]. Nature, 1976, 264(5582): 167-169.
[9] EITZINGER B, EDERER G. The use of nonlinear constitutive equations to evaluate draw resistance and filter ventilation[J]. Beiträge zur Tabakforschung International/Contributions to Tobacco Research, 2014, 19(4): 177-188.
[10] WANG Le, LI Bin, LU Duanfeng, et al. Numerical simulation of dynamic ventilation characteristics of cigarettes under different smoking conditions[J]. Tobacco Science & Technology, 2016, 49(1): 60-65.

[11] YU Qichang, WU Junzhang, HUANG Yifei, et al. Influencing factors of cigarette diffusion process simulation based on CFD[J]. Tobacco Science and Technology, 2017, 50(5): 73-78.
[12] GUGAN K. Natural smolder in cigarette[J]. Combustion and Flame, 1966: 161-164.
[13] MURAMATSU M, UMEMURA S, OKADA T. A mathematical model of evaporation/pyrolysis processes inside a naturally smoldering cigarette[J]. Combust and Flame. 1979, 36: 245-262.
[14] YAN Cong, XIE Wei, LI Yuefeng, et al. Numerical simulation of cigarette smoldering process[J]. Tobacco Science and Technology, 2014, 47(6): 15-20, 37.
[15] CHEN P. Mathematical model of cigarette smoldering process[J]. Beiträge Zur Tabakforschung International/Contributions to Tobacco Research, 2002, 20(4): 265-271.
[16] CHEN Qiuping, XIE Guowei, LUO Wei, et al. Preparation of eicosane/expanded graphite composite phase change material and its regulation of cigarette filter temperature[J]. Tobacco Science and Technology, 2017, 50:65-72.
[17] WANG Xuanze, YI Jinping, YANG Guangyuan, et al. High-precision multi-point real-time temperature measurement of cigarette filter[J]. Journal of Hubei University of Technology, 2023,38(05):9-13.
[18] CUI Ting, WANG Juanjuan, LI Xiaofu, et al. Effect of temperature on the accuracy of cigarette smoking resistance and ventilation rate measurement[J]. China Testing, 2021,47(S2):186-190.
[19] SHI Chunxin, ZHENG Xudong, WU Jiande, et al. Temperature field analysis and experimental study of heating element for heated cigarettes[J]. Tobacco Science and Technology,2020,53(11):89-96.
[20] LIU Hanqing. Hydrodynamic simulation of cigarette flue gas filtration[D]. Dalian: Dalian University of Technology,2021.
[21] WANG Le, YOU Min, CUI Xiaomeng, et al. Cigarette smoking resistance and ventilation characteristics prediction method based on linear network model [J]. Tobacco Science & Technology,2017,50(12):85-89.
[22] LI B, CUI X M, ZHAO L C, et al. Pressure and gas flow distribution inside the filter of a Non-Filter ventilated lit cigarette during puffing [J]. Beiträge zur Tabakforschung International, 2017, 27(6): 113-124.